# Direct Modulation and Free-Space Transmissions of up to 6 Gbps Multilevel Signals With a 4.65-$\mu$m Quantum Cascade Laser at Room Temperature

Xiaodan Pang, *Senior Member, IEEE*, Richard Schatz, Mahdieh Joharifar, Aleksejs Udalcovs, *Senior Member, IEEE*, Vjaceslavs Bobrovs, Lu Zhang, Xianbin Yu, *Senior Member, IEEE*, Yan-Ting Sun, Gregory Maisons, Mathieu Carras, Sergei Popov, *Fellow, IEEE*, Sebastian Lourdudoss, *Senior Member, IEEE*, and Oskars Ozolins, *Member, IEEE*

***Abstract*—A roadmap for future wireless communications is expected to exploit all transmission-suitable spectrum bands, from the microwave to the optical frequencies, to support orders of magnitude faster data transfer with much lower latency than the deployed solutions nowadays. The currently under-exploited mid-infrared (mid-IR) spectrum is an essential building block for such an envisioned all-spectra wireless communication paradigm. Free-space optical (FSO) communications in the mid-IR region have recently attracted great interest due to their intrinsic merits of low propagation loss and high tolerance of atmospheric perturbations. Future development of viable mid-IR FSO transceivers requires a semiconductor source to fulfill the high bandwidth, low energy consumption, and small footprint requirements. In this context, quantum cascade laser (QCL) appears as a promising technological choice. In this work, we present an experimental demonstration of a mid-IR FSO link enabled by a 4.65-$\mu$m directly modulated (DM) QCL operating at room temperature. We achieve a transmission data rate of up to 6 Gbps over a 0.5-m link distance. This achievement is enabled by system-level characterization and optimization of transmitter and receiver power level and frequency response and assisted with advanced modulation and digital signal processing (DSP) techniques. This work pushes the QCL-based FSO technology one step closer to practical terrestrial applications, such as the fixed wireless access and the wireless mobile backhaul. Such a QCL-based solution offers a promising way towards the futuristic all-spectra wireless communication paradigm by potentially supporting the whole spectrum from the MIR to the terahertz (THz).**

***Index Terms*—Free-space communication, quantum cascade laser, mid-infrared photonics.**

Manuscript received September 23, 2021; revised December 10, 2021; accepted December 21, 2021. Date of publication December 23, 2021; date of current version April 18, 2022. This work was supported in part by the Swedish Research Council (VR) projects under Grants 2019-05197 and 2016-04510, in part by the EU H2020 Project cFLOW under Grant 828893, in part by the COST (European Cooperation in Science and Technology) through COST Action under Grant CA19111 NEWFOCUS, and in part by the ERDF-funded CARAT project under Grant 1.1.1.2/VIAA/4/20/660. *(Corresponding author: Xiaodan Pang.)*

Xiaodan Pang is with the Applied Physics Department, KTH Royal Institute of Technology, 106 91 Stockholm, Sweden, and also with the Networks Unit, RISE Research Institutes of Sweden, 164 40 Kista, Sweden (e-mail: xiaodan@kth.se).

Richard Schatz, Mahdieh Joharifar, Yan-Ting Sun, Sergei Popov, and Sebastian Lourdudoss are with the Applied Physics Department, KTH Royal Institute of Technology, 106 91 Stockholm, Sweden (e-mail: rschatz@kth.se; mahdieh@kth.se; yasun@kth.se; sergeip@kth.se; slo@kth.se).

Aleksejs Udalcovs is with the Networks Unit, RISE Research Institutes of Sweden, 164 40 Kista, Sweden (e-mail: aleksejs.udalcovs@gmail.com).

Vjaceslavs Bobrovs is with the Institute of Telecommunications, Riga Technical University, 1048 Riga, Latvia (e-mail: vjaceslavs.bobrovs@rtu.lv).

Lu Zhang and Xianbin Yu are with the College of Information Science and Electronic Engineering, Zhejiang University, Hangzhou 310027, China, and also with the Zhejiang Lab, Hangzhou 310000, China (e-mail: zhanglu1993@zju.edu.cn; xyu@zju.edu.cn).

Gregory Maisons and Mathieu Carras are with mirSense, Centre d'intégration NanoInnov, 91120 Palaiseau, France (e-mail: gregory.maisons@mirsense.com; mathieu.carras@mirsense.com).

Oskars Ozolins is with the Applied Physics Department, KTH Royal Institute of Technology, 106 91 Stockholm, Sweden, with the Networks Unit, RISE Research Institutes of Sweden, 164 40 Kista, Sweden, and also with the Institute of Telecommunications, Riga Technical University, 1048 Riga, Latvia (e-mail: ozolins@kth.se).

Color versions of one or more figures in this article are available at https://doi.org/10.1109/JLT.2021.3137963.

Digital Object Identifier 10.1109/JLT.2021.3137963

## I. Introduction

TO ACCOMMODATE the exponentially increasing data traffic in our digital society, the fifth generation (5G) wireless communication networks currently being deployed have opened up the spectrum in the sub-6 GHz and the millimeter-wave (mmWave) bands. Following such a trend, it is foreseeable that more electromagnetic (EM) spectral regions will be utilized for wireless communications beyond the 5G, including the terahertz (THz) band (0.1–10 THz) and the optical frequencies (infrared, visible and ultraviolet). Such a new paradigm, so-called all-spectra communications, offers the possibility to create a sustainable technology roadmap beyond the next generations of wireless communications [1]. Free-space optical communication (FSO) is expected to play a vital role in unlocking many current limitations inside the scope of this all-spectra communication paradigm. The FSO, spanning from the infrared to the ultraviolet, offers abundant spectral resources and development opportunities. Moreover, these unlicensed spectrum windows can potentially offer extra spectral resources and complementary propagation properties for future wireless applications, with similar high-directional properties with the extensively studied mmWave and THz technologies [2]. FSO technologies have been proposed, studied, and even developed since decades ago by reusing the fiber-optic components in the near-infrared (NIR) band (1–2 $\mu$m). Unfortunately, these have not been considered as reliable building blocks of the modern

ICT infrastructure. The main concern of these NIR FSO technologies is that they are susceptible to the dynamic atmospheric environment. Recently, the under-exploited mid-infrared (MIR) spectral region, in particular the two atmospheric transmission windows at the mid-wavelength IR (MWIR, 3–5 $\mu$m) and the long-wavelength IR (9–12 $\mu$m), are attracting increasing interest for FSO communications, owing to their intrinsic merits of better robustness against various weather conditions, for instance, scattering by aerosols, rain, and snow, as well as beam broadening and scintillation by turbulence effects, compared with the NIR FSO [3].

Several MIR FSO transmission demonstrations have been reported based on the wavelength conversion approaches, which up-convert the optical wavelength at the transmitter and down-convert it at the receiver [4]–[7]. Based on such a nonlinear process, up to 10 Gbps single-channel transmissions are demonstrated with in-phase and quadrature (IQ) modulated signals [8], [9]. Very recently, by extending this approach with multi-dimensional multiplexing techniques, MIR FSO transmissions with an aggregated data rate of up to 300 Gbps are demonstrated [10]. However, its inherent hardware complexity and high power consumption can hinder its practical development, compared with the highly integrable semiconductor transceiver technologies developed for fiber-optic and wireless communication systems. Therefore, it is essential to identify a viable semiconductor technology easily miniaturized with low power consumption for practical MIR FSO transceiver development.

Quantum cascade laser (QCL), which can cover the MIR to the THz range by exploiting inter-subband transitions [11], [12], has appeared promising for MIR FSO transceivers. The later breakthrough in continuous-wave (CW) and room-temperature operation further enhanced the potential of applying QCLs for communication systems [13]. Particularly, directly modulated (DM) QCLs can benefit from their intrinsic high modulation bandwidth, resulting from their short carrier relaxation lifetime, making the laser response over-damped leading to the suppression of a resonance frequency [14], [15]. Several DM QCL-based FSO transmissions have been demonstrated since the early 2000s [16]–[20]. However, practical shortcomings in one or more aspects limited their further development. More specifically, these works either were demonstrated at cryogenic temperatures to support digital binary transmission of up to a few Gbps [16] or were limited to a few hundreds of MHz analog signal bandwidth with Peltier cooling [20]. Similar MIR-FSO demonstrations were also reported with directly modulated interband cascade lasers (ICL), with data rates limited to a few tens of Mbps [21]. In recent years, high bandwidth modulation of QCLs at room-temperature has been made possible [22], [23], which has prompted renewed interest in studying QCL-based FSO systems. Lately, a few QCL-based FSO demonstrations are reported for both classical and private free-space communications [24]–[26]. Besides the DM QCL-based schemes, MIR-FSO based on external modulation has also emerged as a promising alternative. For example, up to 10 Gbps binary data transmissions at 9 $\mu m$ have been demonstrated recently with a large bandwidth amplitude modulator [27], indicating great potential for further explorations.

On top of it, it has been a common practice for digital communication systems, both in fiber-optics and wireless, to employ advanced modulation, digital signal processing (DSP), and coding techniques to realize capacity-approaching transmission performances. In this aspect, the state-of-the-art includes modulation and detection of up to 4 Gbps pulse amplitude modulation (PAM) and discrete multi-tone (DMT) signals that are directly modulated with a MIR QCL operating at room temperature, enabled by effective digital equalizations [28], [29]. Yet, the reported transmission distance was limited to 5 cm due to the receiver's low signal-to-noise ratio (SNR) without proper beam collimation.

In this paper, we extend our preliminary results recently reported in [30] and explain in detail the digital pre- and post-equalization methods, as well as show additional experimental results. We show our improved MIR FSO transmission demonstration with a 4.65-$\mu$m DM QCL and a bandwidth-limited commercial mercury cadmium telluride (MCT) photovoltaic MIR detector. The QCL is operated at room temperature in this demonstration, and proper collimation is configured on the laser mount. The transmission distance is increased to 0.5 m, with a substantial extra power margin for further extension. We perform a thorough exploration of the system limit with three modulation formats, namely, non-return-to-zero on-off-keying (NRZ-OOK), PAM4, and PAM8, both with and without digital post-equalizations. Without any post equalizations, we demonstrate that up to 1.6 Gbps data rate with NRZ-OOK signal is achievable with a bit error rate (BER) below the 6.7% overhead (OH) hard-decision FEC (HD-FEC) limit. Furthermore, with effective digital post-equalizers applied, up to 6 Gbps PAM8 signals are transmitted over the bandwidth-limited link and successfully received below the same FEC threshold. To the best of our knowledge, this work presents the highest reported bit-rate distance product of DM QCL-based MIR FSO transmission at room temperature.

## II. System Configuration and Characterization

### *A. Experimental Setup of the QCL-Based FSO Transmission System*

The QCL-based mid-IR FSO transmission system is demonstrated experimentally with a tabletop setup, as shown in Fig. 1. The three modulation formats under test, NRZ-OOK, PAM4, and PAM8, are generated offline with a transmitter-side (Tx) digital signal processing (DSP) routine at a lab computer. The Tx DSP routine consists of a PAM mapper where a repeated pseudorandom binary sequence of the word length of $2^{15}-1$ (PRBS-15) is mapped to the PAM symbols. Such a word length is chosen to avoid any deterministic patterning effects occurring with shorter bit sequences, e.g. PRBS-7 or PRBS-9, resulting in over-optimistic transmission performances at high bit rates. The generated PAM symbols are then pulse shaped with a raised cosine filter of 0.15 roll-off factor and re-sampled to match the sampling rate of the arbitrary waveform generator (AWG). Before loading the signal to the AWG, we applied a simple static pre-emphasis filter to pre-compensate the system bandwidth limitation. The details of the pre-emphasis processing

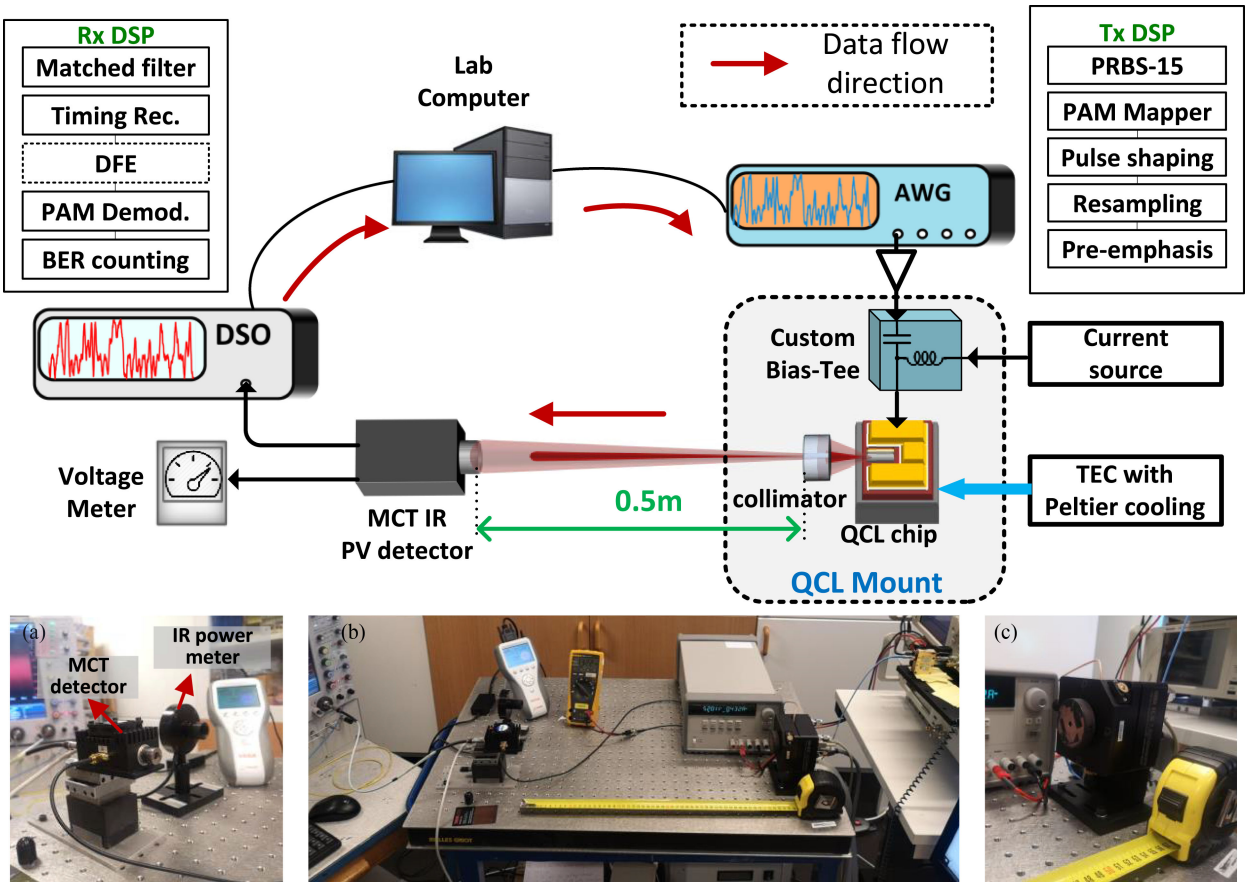


Fig. 1. Experimental setup with the configuration details of transmitter and receiver DSP. PRBS: pseudorandom binary sequence; AWG: arbitrary waveform generator; TEC: temperature controller; MCT: mercury cadmium telluride; DSO: digital storage oscilloscope; DFE: decision-feedback equalizer. The photos of the IR power meter and the MCT receiver, the link, and the QCL mount are shown in insets (a), (b), and (c), respectively.

is described in Section II-C. The digital signals after the Tx DSP are converted to the analog domain by the AWG, which has a 3-dB bandwidth of 12 GHz and operates at 50 GSa/s to avoid aliasing. In practice, with an anti-aliasing filter, a lower sampling rate of around 8 GSa/s is sufficient to support the demonstrated data rates in this experiment.

The output signals from the AWG are electrically amplified to at least 2.5 $V_{peak-to-peak}$ by a linear driver amplifier. The amplitude of the driving signals is varied between different baud rates and modulation formats for performance optimization. A custom-made bias tee is used to deliver the modulation signal and the laser bias current to the QCL chip under test. The QCL chip is fabricated by mirSense, a distributed feedback (DFB) laser model from a previously reported design, and has a center wavelength of 4.65-$\mu$m [22]. The laser chip and the bias tee are mounted on a commercial QCL mount (ILX Lightwave LDM-4872) with a Peltier temperature controller (TEC) and a water-cooled base. A beam collimating lens installed at the QCL mount is used to collimate the high-divergence optical beam emitted from the QCL chip. The highly directive mid-IR signal is transmitted over a 0.5-m distance, which is chosen due to the tabletop space constraint and local laser safety regulations. At the receiver, we firstly calibrate the received signal power with an IR power meter, and the calibration results are further detailed in Section II-B. Later, we replace the IR power meter with a commercial MCT (HgCdTe) photovoltaic MIR PD for the transmission measurements. The picture of the IR power meter and the MCT PD are shown in Fig 1(a). The PD is mounted in a thermo-electrically cooled module and has a built-in trans-impedance amplifier (TIA). The 3-dB bandwidth of the MCT PD as per the manufacture's specification is around 720 MHz.

The received signal is converted to digital samples at a real-time digital storage oscilloscope (DSO) operating at 10 GSa/s. We collect the converted digital traces at the lab computer and perform a receiver-side (Rx) DSP routine offline to recover the transmitted data. The Rx DSP consists of a matched filter, timing recovery, a symbol-spaced adaptive decision-feedback equalizer (DFE), and symbol demodulation. In the end, the recovered data sequence is compared with the transmitted data for bit error rate (BER) computation. Each received signal trace consists of 520 k symbols for BER calculation.

### B. *Device and Subsystem Characteristics*

We first characterize the power and frequency response of the combined QCL and MCT MIR PD subsystem. The measured P-I curve of the QCL is shown in Fig. 2(a). The QCL under CW operation has a lasing threshold of 178 mA at a temperature of

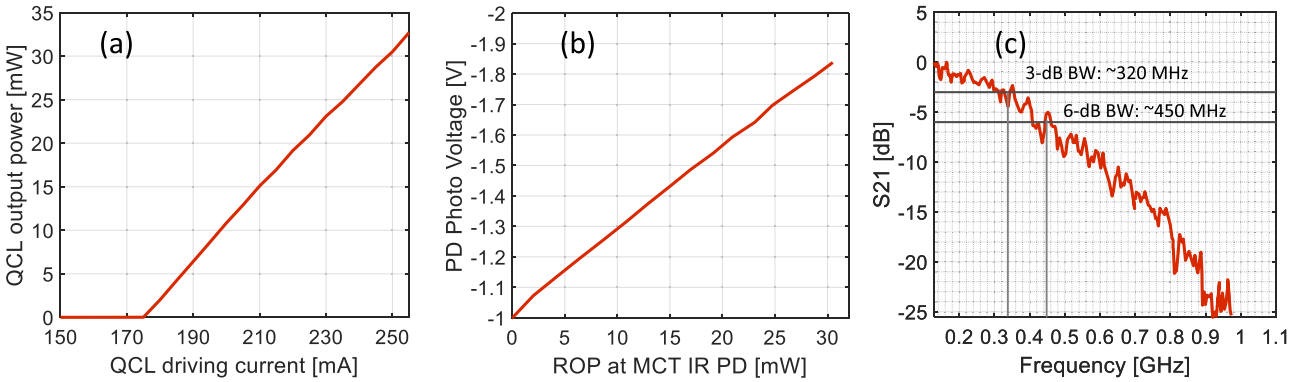


Fig. 2. (a) The output power of the QCL under CW operation as a function of driving current. (b) The MCT IR PD PV as a function of the received optical power (ROP). (c) End-to-end S21 characteristics measured at optimum received optical power level.

292 K (19 °C). To prevent potential damage to the QCL chip from overdriving, we measured with a laser bias current of up to 255 mA, at which the QCL has an output power of 32.7 mW. Since no sign of output saturation is observed at this power level, we keep the laser operating at this bias point during all transmission measurements.

As shown in later sections that the signal transmission performances are measured with respect to the photovoltage (PV) of the MCT MIR PD, we perform power calibration measurement of the receiver. The calibration result is shown in Fig. 2(b). It is observed that the absolute PV value of the MCT PD increases linearly with the received optical power across the range of measurement.

Finally, we use a vector network analyzer (VNA) to characterize the end-to-end frequency response of the system from the QCL input to the MCT PD output. During the measurements, we observe that the system bandwidth is correlated with the laser power, and increasing the power beyond an optimal value causes a decrease in bandwidth. Such a bandwidth-power correlation may be attributed to the known fact that the QCL modulation bandwidth often varies with the laser bias [31] or further partly due to the detector saturation. In our configuration, the optimal received optical power (ROP) is found to be 10 mW, corresponding to a detector PV of 1.3 V. Fig. 2(c) shows the characterized system bandwidth at the optimum received power level. The end-to-end 3-dB bandwidth is found to be around 320 MHz, and 6-dB bandwidth is around 450 MHz. The current system bandwidth is most likely limited by the MCT MIR PD and the electrical parasitic in the laser mount, which is to be verified systematically in our next-step studies when a broader bandwidth detector is available.

### C. The Transmitter Pre-Emphasis Filter Configuration

Fig. 2(c) shows that the limited end-to-end system bandwidth can impose strong frequency roll-off of the transmitted signals at gigabit data rates. To pre-compensate such frequency roll-off, we apply a low-complexity 2-tap pre-emphasis finite impulse response (FIR) filter at the transmitter right before the digital-to-analog conversion. The Z-domain transfer function of the filter is $H_{pre-emphasis}(Z) = 1 + \alpha Z^{-1}$, where $\alpha$ is the pre-emphasis coefficient ranging from 0 to $-1$. When $\alpha = 0$, there is no pre-emphasis, and $\alpha = -1$ corresponds to a maximum pre-emphasis with a substantial enhancement of the high-frequency response. Fig. 3(a) shows the magnitude frequency response of the pre-emphasis filter at the transmitter with different $\alpha$ values. In our transmission experiments, the pre-emphasis coefficient $\alpha$ is kept at $-0.99$ to ensure an effective pre-compensation of the frequency roll-off of the broadband signals. The generated eye diagrams for NRZ-OOK, PAM4, and PAM8 before and after the pre-emphasis filtering are shown in Fig. 3(b)–(g). It is observed that the pre-emphasis filter pre-distorts the signal and induces eye closure at the transmitter. Yet, it improves the overall transmission performance after the strong filtering imposed by the FSO link.

## III. System Transmission Results

After characterizing the power and frequency performance of the QCL-based transmitter and MCT receiver, we continue evaluating the system transmission performance with the previously mentioned three modulation formats, i.e., NRZ-OOK, PAM4, and PAM8. For each modulation format under test, we explore the highest bit rates with achievable BER against two hard-decision FEC thresholds, i.e., the 6.7%-OH staircase HD-FEC limit of 4.5E-3 and the KP4-FEC limit of 2.2E-4. [32], [33] One should note that these two FEC thresholds are only adopted for performance benchmarking, and more specific FEC codes should be applied in practice.

### A. Transmission Performance of NRZ-OOK Signals With and Without Digital Post-Equalization

Firstly, we evaluate the system-supported data rate without digital post-equalizers, which may be favored in specific time-sensitive applications. In our experiment, only the NRZ-OOK signal format can be successfully demodulated without post-equalization. In contrast, the vertical eye openings of the unequalized PAM4 and PAM8 signals are undetectable for the targeted BER thresholds. The highest achievable baud rates for unequalized NRZ-OOK to reach below the 2.2E-4 and the

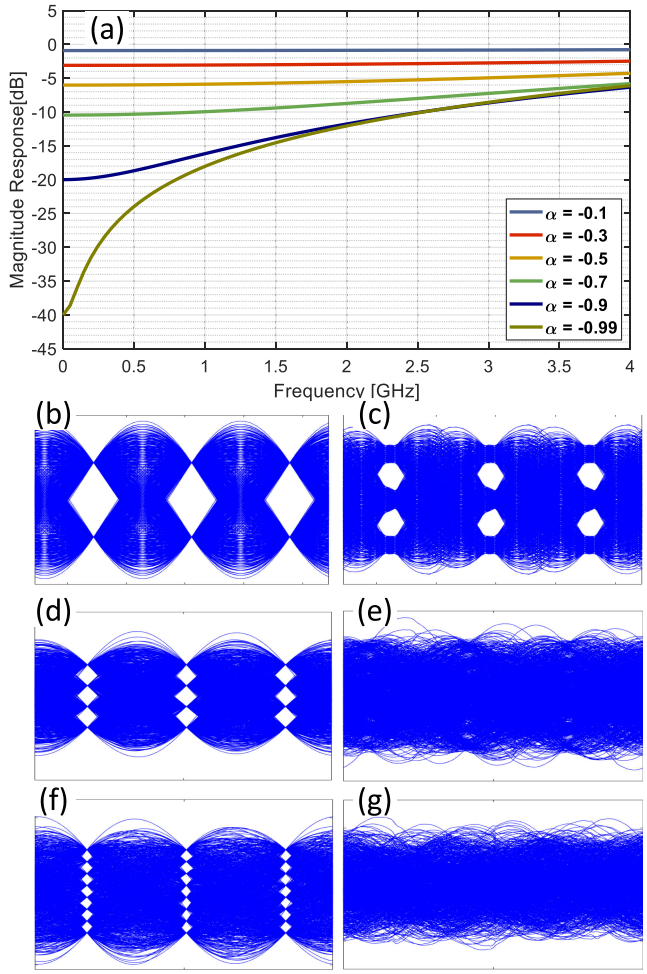


Fig. 3. (a) The frequency response of the pre-emphasis FIR filter in magnitude with different pre-emphasis coefficient $\alpha$ values; (b)–(c). Eye diagrams of 4 Gbaud NRZ signal before and after the pre-emphasis filter; (d)–(e). Eye diagrams of 2.5 Gbaud PAM4 signal before and after the pre-emphasis; (f)–(g). Eye diagrams of 2 Gbaud PAM8 signal before and after the pre-emphasis. $\alpha$ was set to -0.99 in the pre-emphasis cases shown in (c), (e) and (g).

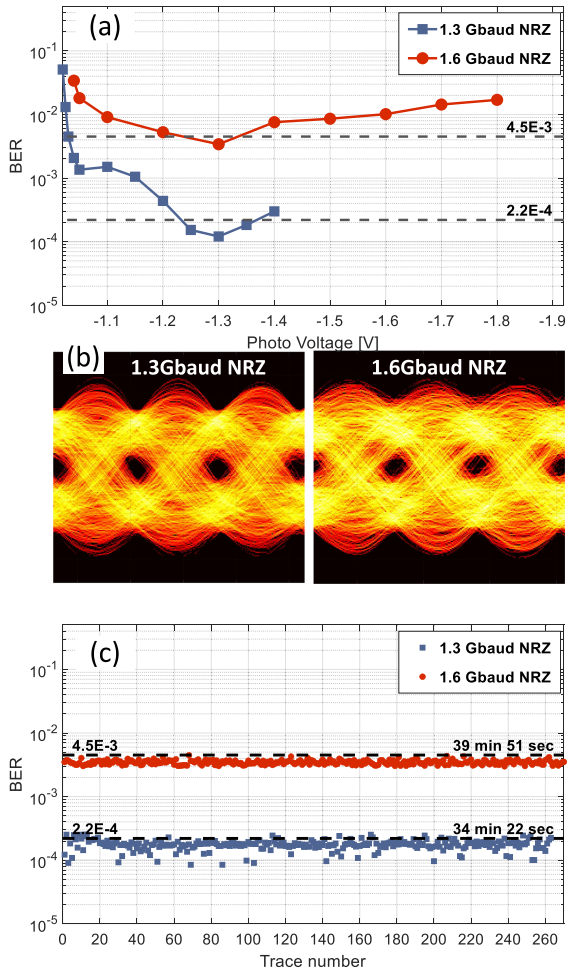


Fig. 4. (a) BER as a function of the detector PV for NRZ-OOK signals without any post digital equalization at 1.3 Gbaud (1.3 Gbps) and 1.6 Gbaud (1.6 Gbps), respectively. (b) Selected eye diagrams for both data rates measured at PV of −1.3 V. (c) System stability test results at both data rates.

4.5E-3 BER limits are 1.3 Gbaud and 1.6 Gbaud, respectively, and the measured BER performance as a function of the detector PV are shown in Fig. 4(a). The optimal PV value where the lowest BER for both data rates is achieved is around −1.3 V or 10 mW ROP. The eye diagrams of the received signals at −1.3 V PV without post-equalization are presented in Fig. 4(b). One can see that despite the inter-symbol-interference (ISI)-induced eye closure, sufficient eye openings are detectable with a properly adjusted decision threshold. Further increase of the ROP degrades the BER performance, mainly due to the bandwidth shrinkage mentioned earlier. Finally, we evaluate the stability performance of the transmission for both data rates and show the results in Fig. 4(c). During this test, the system was kept running at the optimal operation point to capture and process the received data traces in a quasi-real-time manner, and the BER results are plotted on the fly. More than 250 traces with 4 million samples per trace are processed over more than 30 minutes for each data rate. One should note that the time duration of the stability test depends on the time required to transfer and process a trace and this time is different for each modulation format. In this case, only a few outliers with marginally higher BER than the corresponding FEC limits are detected throughout the measurement time due to vibrations, indicating a stable performance for both the DM QCL-based transmitter and the MCT detector.

We then explore the highest supported data rates with NRZ-OOK signal after introducing the digital post equalizers. A symbol-spaced DFE consisting of 33 feed-forward (FF) taps and 33 feedback (FB) taps are applied in the measurements. With effective post-equalization, 3 Gbaud NRZ-OOK signal can reach below the KP4-FEC limit, and the HD-FEC limit can be achieved at 4 Gbaud. Fig. 5(a) shows the measured BER results for NRZ-OOK signals for both baud rates. We find that the optimal PV range for both baud rates is between −1.2 V and −1.4 V, which corresponds to the ROP of between 5.2 mW and 11 mW. The equalized signal eye diagrams at −1.2 V for both baud rates are shown in Fig. 5(b). Clear eye openings are achieved thanks to sufficient receiver SNR and effective equalization. Fig. 5(c)

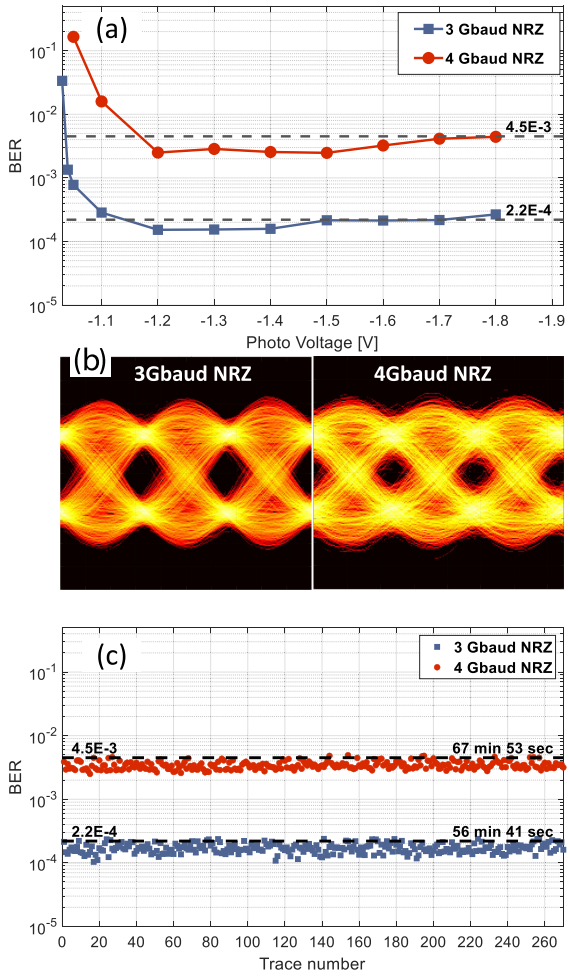


Fig. 5. (a) BER as a function of the detector PV for NRZ-OOK signals at 3 Gbaud (3 Gbps) and 4 Gbaud (4 Gbps), respectively. (b) Selected eye diagrams for both data rates measured at PV of −1.2 V. (c) System stability test results at both data rates.

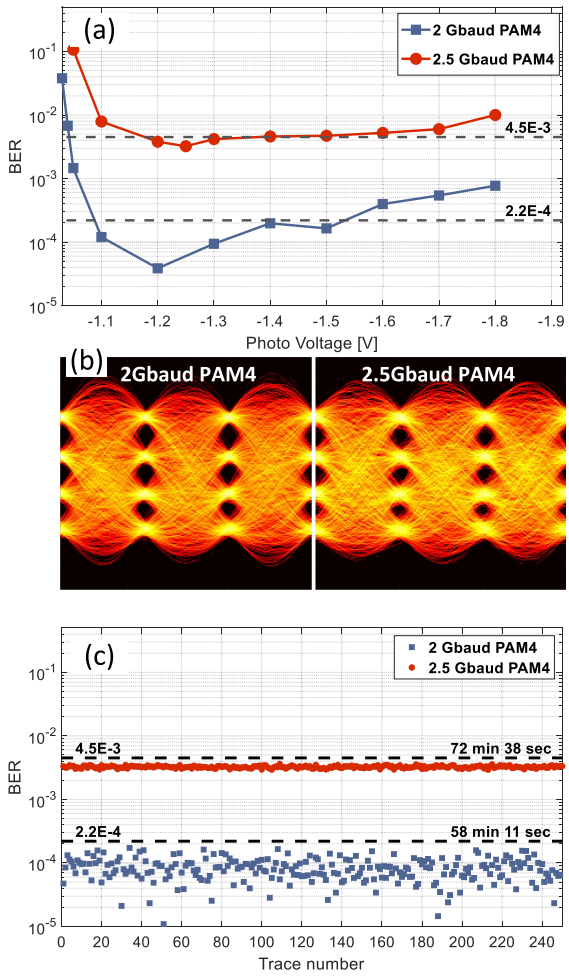


Fig. 6. (a) BER as a function of the detector PV for PAM4 signals at 2 Gbaud (4 Gbps) and 2.5 Gbaud (5 Gbps), respectively. (b) Selected eye diagrams for both data rates measured at their respective optimal PV values. (c) System stability test results at both data rates.

presents the system stability test results operating at −1.2 V PV. Similarly, stable BER performances are observed for both data rates over 260 data traces, collected during around 1 h period for each case.

### *B. Transmission Performance of PAM4 Signals*

We switch to the PAM4 signal format with the same system configuration to explore the supported data rates against the two benchmarking FEC thresholds. The corresponding BER performances are also measured accordingly. The same DFE configuration as the NRZ-OOK case is adopted. 2 Gbaud and 2.5 Gbaud PAM4 signals are successfully transmitted and received through the MIR FSO link to reach below the respective KP4- and HD-FEC limits, corresponding to raw data rates of 4 Gbps and 5 Gbps. We plot the BER curves for the PAM4 signals at these two baud rates in Fig. 6(a). The optimal detector PV for 2 Gbaud PAM4 was around −1.2 V, and for 2.5 Gbaud around −1.25 V. For the PAM4 cases, we observe a slightly steeper BER degradation compared with NRZ-OOK when increasing the received power beyond the optimal values. This observation can be attributed to the additional impairment caused by the MCT detector TIA saturation, which affects the system linearity required by higher-order PAM signals. The eye diagrams for PAM4 signals detected at their optimal ROP for both baud rates are shown in Fig. 6(b). Though slight eye compression is observed at 2.5 Gbaud, satisfying BER performances are guaranteed with clear and adequately wide eye openings in both cases. Similarly, the system stability tests for PAM4 at both data rates are performed at their respective optimal operation points. As seen in Fig. 6(c), no single outlier point crossing the corresponding FEC limits is detected over the ∼1-hour duration for both data rate cases.

### *C. Transmission Performance of PAM8 Signals*

Finally, we employ the PAM8 signal format to explore the system limit further. For an effective equalization, a DFE with 55 FF taps and 55 FB taps is used in the PAM8 cases. 1.5 Gbaud and 2 Gbaud PAM8 signals, corresponding to raw data rates of 4.5 Gbps and 6 Gbps, are found to be achievable against the KP4- and HD-FEC limits, respectively. Fig. 7(a) shows the BER

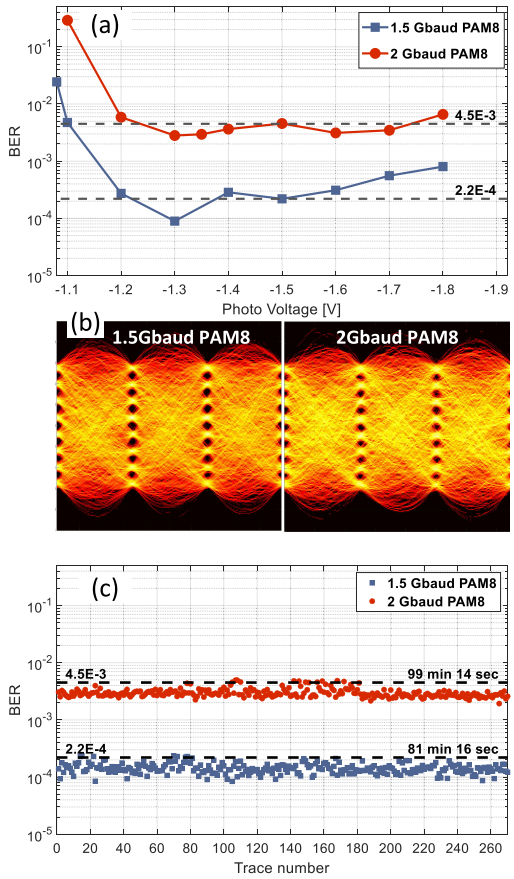


Fig. 7. (a) BER as a function of the detector PV for PAM8 signals at 1.5 Gbaud (4.5 Gbps) and 2 Gbaud (6 Gbps), respectively. (b) Selected eye diagrams for both data rates measured at their respective optimal PV values. (c) System stability test results at both data rates.

performance for the PAM8 signals measured against the MCT detector PV. An optimal detector PV of −1.3 V is identified for both baud rates, considering the trade-offs among the required signal SNR, the system linearity, and the detector bandwidth. As shown in Fig. 7(b), clear eye openings are again observed after equalization at both baud rates, indicating a low-noise and high-linearity performance of the MIR FSO system, particularly the DM QCL-based transmitter. Fig. 7(c) presents the measured system stability when operating with the PAM8 signals. Longer processing time is required compared with NRZ-OOK, and PAM4, due to the increased number of bits carried with the same number of samples per data trace, resulting in more than 80 minutes of testing duration for each data rate. Again, stable BER performances are kept throughout the measurements, with only a few outlier cases marginally crossing the corresponding FEC thresholds.

## IV. Conclusion

In this work, we have demonstrated a directly modulated QCL-based MIR FSO link with three amplitude modulation formats, i.e., NRZ-OOK, PAM4, and PAM8, operating at room temperature. Without any post-equalization, successful transmissions of NRZ-OOK signals of 1.3 Gbps and 1.6 Gbps are achieved with BER performances below the KP4-FEC and the 6.7%-OH HD-FEC limits, respectively. Assisted with effective post equalization techniques, up to 4.5 Gbps data rate to meet the KP4-FEC threshold and up to 6 Gbps data rate to reach the HD-FEC threshold are successfully demonstrated over the 0.5-m MIR FSO link. Enabled by proper beam collimation, thus the enhanced receiver SNR, this demonstration shows a 50% higher achievable data rate with ten times longer reach than the previous record of 4 Gbps data rate over 5 cm link distance. Since the atmospheric attenuation at this wavelength window is below 1 dB/km [3] and the power margin of the current MIR FSO setup is considerably large, we can confidently expect a much longer transmission distance at the same data rates for all three tested modulation formats with ideal alignment and beam collimation. Therefore, in the near term, we plan to take extra laser safety measures and make further research efforts towards higher data rates and longer-distance transmissions in the MIR region. In the mid to long term, research towards the all-spectra communication paradigm by opening the spectrum window from the MIR to the THz can be well-envisioned with such QCL-based technologies. The optimal choice of modulation formats in this spectral region will also need to be explored by jointly considering the tradeoff between the bandwidth and the SNR, as well as the propagation characteristics of the dynamic atmospheric channel. Furthermore, with the recent research progress in ultrafast mid-IR photodetectors [34], [35] and high-speed modulation of room-temperature THz QCLs [36], [37], orders of magnitude higher transmission data rates crossing the MIR to the THz region can be expected by extending the system-level methodologies of this work. These topics will be the focus of our next-phase explorations.

## Acknowledgment

The authors would like to thank Joakim Storck and Danya Mohamad for initial QCL mounting and characterization.

## References

[1] X. You *et al.*, "Towards 6G wireless communication networks: Vision, enabling technologies, and new paradigm shifts," *Sci. China Inf. Sci.*, vol. 64, no. 1, pp. 1–74, 2020.
[2] M. A. Khalighi and M. Uysal, "Survey on free space optical communication: A communication theory perspective," *IEEE Commun. Surveys Tuts.*, vol. 16, no. 4, pp. 2231–2258, Oct./Dec. 2014.
[3] A. Delga and L. Leviandier, "Free-space optical communications with quantum cascade lasers," *Proc. SPIE*, vol. 10926, 2019, Art. no. 1092617.
[4] Q. Hao *et al.*, "Mid-infrared transmitter and receiver modules for free-space optical communication," *Appl. Opt.*, vol. 56, no. 8, pp. 2260–2264, 2017.
[5] E. Ip *et al.*, "QPSK transmission over free-space link at 3.8 $\mu$m using coherent detection with wavelength conversion," in *Proc. 34th Eur. Conf. Opt. Commun.*, 2008, pp. 1–2.
[6] K.-D. F. Büchter, H. Herrmann, C. Langrock, M. M. Fejer, and W. Sohler, "All-optical Ti:PPLN wavelength conversion modules for free-space optical transmission links in the mid-infrared," *Opt. Lett.*, vol. 34, no. 4, pp. 470–472, 2009.
[7] P. Cho *et al.*, "Optical homodyne RZ-QPSK transmission through wind tunnel at 3.8 and 1.55 micron via wavelength conversion," *Proc. SPIE*, vol. 7324, 2009, Art. no. 73240A-1.
[8] Y. Su *et al.*, "10 Gbps DPSK transmission over free-space link in the mid-infrared," *Opt. Express*, vol. 26, no. 26, pp. 34515–34528, 2018.
[9] W. Wang *et al.*, "5 Gbaud QPSK coherent transmission in the mid-infrared," *Opt. Commun.*, vol. 466, 2020, Art. no. 125681.

[10] K. Zou *et al.*, "Demonstration of free-space 300-Gbit/s QPSK communications using both wavelength- and mode- division-multiplexing in the mid-IR," in *Proc Opt. Fiber Commun. Conf. Exhib.*, 2021, pp. 1–3.
[11] J. Faist, F. Capasso, D. L. Sivco, C. Sirtori, A. L. Hutchinson, and A. Y. Cho, "Quantum cascade laser," *Science*, vol. 264, no. 5158, pp. 553–556, 1994.
[12] J. Faist *et al.*, "Distributed feedback quantum cascade lasers," *Appl. Phys. Lett.*, vol. 70, no. 20, pp. 2670–2672, 1997.
[13] M. Beck *et al.*, "Continuous wave operation of a mid-infrared semiconductor laser at room temperature," *Science*, vol. 295, no. 5553, pp. 301–305, 2002.
[14] N. Mustafa, L. Pesquera, C. Y. L. Cheung, and K. A. Shore, "Terahertz bandwidth prediction for amplitude modulation response of unipolar intersubband semiconductor lasers," *IEEE Photon. Technol. Lett.*, vol. 11, no. 5, pp. 527–529, May 1999.
[15] F. Capasso *et al.*, "Quantum cascade lasers: Ultrahigh-speed operation, optical wireless communication, narrow linewidth, and far-infrared emission," *IEEE J. Quantum Electron.*, vol. 38, no. 6, pp. 511–532, Jun. 2002.
[16] R. Martini *et al.*, "High-speed digital data transmission using mid-infrared quantum cascade lasers," *Electron. Lett.*, vol. 37, no. 21, pp. 1290–1292, 2001.
[17] R. Martini *et al.*, "High-speed modulation and free-space optical audio/video transmission using quantum cascade lasers," *Electron. Lett.*, vol. 37, no. 3, pp. 191–193, 2001.
[18] R. Martini *et al.*, "Free-space optical transmission of multimedia satellite data streams using mid-infrared quantum cascade lasers," *Electron. Lett.*, vol. 38, no. 4, pp. 181–183, 2002.
[19] S. Blaser, D. Hofstetter, M. Beck, and J. Faist, "Free-space optical data link using peltier-cooled quantum cascade laser," *Electron. Lett.*, vol. 37, no. 12, pp. 778–780, 2001.
[20] M. Taslakov, V. Simeonov, and H. van den Bergh, "Line-of-sight data transmission system based on mid IR quantum cascade laser," *Proc. SPIE*, vol. 6877, 2008, Art. no. 68770F.
[21] A. Soibel *et al.*, "Midinfrared interband cascade laser for free space optical communication," *IEEE Photon. Technol. Lett.*, vol. 22, no. 2, pp. 121–123, Jan. 2010.
[22] M. Carras *et al.*, "Room-temperature continuous-wave metal grating distributed feedback quantum cascade lasers," *Appl. Phys. Lett.*, vol. 96, no. 16, 2010, Art. no. 161105.
[23] Y. H. Zhou *et al.*, "High-speed quantum cascade laser at room temperature," *Electron. Lett.*, vol. 52, no. 7, pp. 548–549, 2016.
[24] J. J. Liu *et al.*, "Mid and long-wave infrared free-space optical communication," *Proc. SPIE*, vol. 11133, 2019, Art. no. 1113302.
[25] O. Spitz *et al.*, "Private communication with quantum cascade laser photonic chaos," *Nature Commun.*, vol. 12, no. 1, 2021, Art. no. 3327.
[26] O. Spitz *et al.*, "Free-space communication with directly modulated mid-infrared quantum cascade devices," *IEEE J. Sel. Topics Quantum Electron.*, vol. 28, no. 1, pp. 1–9, Jan./Feb. 2022.
[27] H. Dely *et al.*, "10 Gbit/s free space data transmission at 9 $\mu$ m wavelength with unipolar quantum optoelectronics," *Laser Photonics Reviews*, 2021, [online] Available: https://doi.org/10.1002/lpor.202100414.
[28] X. Pang *et al.*, "Gigabit free-space multi-level signal transmission with a mid-infrared quantum cascade laser operating at room temperature," *Opt. Lett.*, vol. 42, no. 18, pp. 3646–3649, 2017.
[29] X. Pang *et al.*, "Free-space communications enabled by quantum cascade lasers," *Physica Status Solidi (a)*, vol. 218, no. 3, 2021, Art. no. 2000407.
[30] X. Pang *et al.*, "Up to 6 Gbps mid-infrared free-space transmission with a directly modulated quantum cascade laser," in *Proc. Eur. Conf. Opt. Commun.*, 2021, pp. 1–4.
[31] A. Calvar *et al.*, "High frequency modulation of mid-infrared quantum cascade lasers embedded into microstrip line," *Appl. Phys. Lett.*, vol. 102, no. 18, 2013, Art. no. 181114.
[32] "OTU4 long-reach interface," ITU-T Recommendation G.709.2/Y.1331.2, 2018.
[33] *IEEE Standard for Ethernet Amendment 2: Physical Layer Specifications and Management Parameters for 100 Gb/s Operation Over Backplanes and Copper Cables*, IEEE Standard 802.3bj-2014 (Amendment to IEEE Std 802.3-2012 as amended by IEEE Std 802.3bk-2013), pp. 1–368, 2014.
[34] D. Palaferri *et al.*, "Room-temperature nine-$\mu$m-wavelength photodetectors and Ghz-frequency heterodyne receivers," *Nature*, vol. 556, no. 7699, pp. 85–88, 2018.
[35] M. Hakl *et al.*, "Ultrafast quantum-well photodetectors operating at 10 m with a flat frequency response up to 70 Ghz at room temperature," *Amer. Chem. Soc. Photon.*, vol. 8, no. 2, pp. 464–471, 2021.
[36] A. Dunn *et al.*, "High-speed modulation of a terahertz quantum cascade laser by coherent acoustic phonon pulses," *Nature Commun.*, vol. 11, no. 1, pp. 1–8, 2020.
[37] A. Khalatpour, A. K. Paulsen, C. Deimert, Z. R. Wasilewski, and Q. Hu, "High-power portable terahertz laser systems," *Nature Photon.*, vol. 15, no. 1, pp. 16–20, 2021.